

Cite this: *Chem. Sci.*, 2022, 13, 1925

All publication charges for this article have been paid for by the Royal Society of Chemistry

Received 7th December 2021
Accepted 13th January 2022

DOI: 10.1039/d1sc06819a

rsc.li/chemical-science

Understanding nascent plasmons and metallic bonding in atomically precise gold nanoclusters†

Xiangsha Du,‡ Zhongyu Liu,  ‡ Tatsuya Higaki, Meng Zhou  and Rongchao Jin *

The metallic bond is arguably the most intriguing one among the three types of chemical bonds, and the resultant plasmon excitation (e.g. in gold nanoparticles) has garnered wide interest. Recent progress in nanochemistry has led to success in obtaining atomically precise nanoclusters (NCs) of hundreds of atoms per core. In this work, thiolate-protected Au₂₇₉(SR)₈₄ and Au₃₃₃(SR)₇₉ NCs, both in the nascent metallic state are investigated by cryogenic optical spectroscopy down to 2.5 K. At room temperature, both NCs exhibit distinct plasmon resonances, albeit the NCs possess a gap (estimated 0.02–0.03 eV, comparable to thermal energy). Interestingly, we observe no effect on plasmons with the transition from the metallic state at r.t. to the insulating state at cryogenic temperatures (down to 2.5 K), indicating a nonthermal origin for electron-gas formation. The electronic screening-induced birth of metallic state/bonding is discussed. The obtained insights offer deeper understanding of the nascent metallic state and covalent-to-metallic bonding evolution, as well as plasmon birth from concerted excitonic transitions.

Introduction

Metallic gold nanoparticles (e.g., 3–100 nm diameter) show elegant surface plasmon resonance (SPR) in the visible wavelength range, which has stimulated great research interest since Faraday's early scientific work in the mid-19th century.^{1–4} In particular, the recent two decades have witnessed intensive research on shape control, hierarchical assembly, and other aspects of nanoparticles, as well as their applications in catalysis, nanoelectronics, optics, sensing and biomedicine.

Toward the smaller end of gold NP sizes (i.e., <3 nm), the SPR gradually fades out with decreasing size due to the quantum size effect,^{5–12} hence, exhibiting a transition from the metallic to the nonmetallic state; the latter is manifested in the emergence of a distinct bandgap or a HOMO–LUMO gap (E_g).^{13–22} On that note, the term 'nonmetallic' is equivalent to molecular, semi-conducting, or insulating, and all of them have been used in the literature. If one starts with the smallest cluster (i.e. diatomic Au₂), the bond in Au₂ is apparently a covalent bond (being nonmetallic), and that in Mg₂ is van der Waals interaction.²³ With increasing number of atoms in the cluster, the E_g value decreases generally (albeit with some local zig-zag behavior²⁴), and over the size range of tens to hundreds of metal atoms the bonding orbitals become more and more closely spaced, ultimately forming a quasi-continuous band (i.e. valence band),

and similarly the antibonding orbitals give rise to the conduction band. When the gap between the two bands is so small, thermal excitation of valence electrons in fully occupied levels into the upper levels becomes predominant and the metallic state is formed.

Theoretically, by setting up the one-electron Schrödinger equation for electrons and ignoring the electron–electron and electron–nuclear interactions (potential energy $V = 0$), one obtains the equation for a single valence electron (mass m) confined in a volume,

$$H\Psi = \left(-\frac{\hbar^2}{2m}\nabla^2 + V \right)\Psi = E\Psi \quad (1)$$

For a cubic system of edge length a , the equation can be readily solved to obtain the energy (E_n) for quantized levels of the electron,

$$E_n = \frac{\hbar^2 \times \varphi^2}{2ma^2} n^2 \quad (2)$$

where $n^2 = n_x^2 + n_y^2 + n_z^2$, and n_x , n_y and n_z are the integer quantum numbers. The $E_n \sim n^2$ relation indeed forms a sphere of radius n (only one octant of the sphere).

For the spherical coordinate system (radius a for the sphere), one can similarly solve the one-electron Schrödinger equation and obtain,

$$E = \frac{\hbar^2}{2ma^2} \alpha_{n,l}^2 \quad (3)$$

where $\alpha_{n,l}$ represents the n^{th} zero of the l^{th} spherical Bessel function of the first kind.

Department of Chemistry, Carnegie Mellon University, Pittsburgh, Pennsylvania 15213, USA. E-mail: rongchao@andrew.cmu.edu

† Electronic supplementary information (ESI) available: Synthesis and characterization, including mass spectrometry (MS) and cryogenic spectroscopy. See DOI: 10.1039/d1sc06819a

‡ These authors contributed equally to this work.



With the discrete values of $n_{x,y,z}$ or $\alpha_{n,l}$, one can construct the energy-level diagram. The average spacing (δ) between successive levels can be estimated from the reciprocal of the density of states according to eqn (2),^{25,26}

$$\delta = \frac{4E_f}{3N} \quad (4)$$

where E_f is the bulk metal's Fermi energy, and N is the total number of valence electrons, which is equal to the total number of gold atoms since gold only contributes one 6s electron. In the case of a sufficiently large number of atoms in the particle, the discrete quantum numbers ($n_{x,y,z}$ in the cubic particle, or (n, l) in the spherical one) become very large. Apparently, the level spacing follows an inverse scaling relation with the size (N) and thus reaches the criterion $E_g = 0$ for a bulk solid being metallic ($N \rightarrow \infty$). However, for a finite system (e.g. NPs), the E_g value never reaches zero, no matter the particle is in the nonmetallic- or metallic-state. Thus, Kubo suggested a metallicity criterion for particles by comparing the E_g with the thermal energy,²⁶ that is,

$$E_g = \delta < k_B T \text{ (Kubo criterion)} \quad (5)$$

where k_B is the Boltzmann constant and T is the thermodynamic temperature in Kelvin. This implies temperature dependence of the metallic state, but it has not been explicitly discussed or experimentally tested over the past few decades.^{27,28} The Kubo criterion has been widely used in the cluster science field, in particular the gas phase bare clusters of metal elements^{29,30} and the metal islands³¹ on substrates. To test the criterion experimentally, well-defined nanoparticles in the nascent metallic state are required, but this has long been a major challenge.

In recent years, solution phase nanochemistry has advanced significantly,² and recent progress has indeed led to the development of atomically precise metal nanoclusters (NCs) protected by ligands.^{10–22} Unlike the gas phase NCs for which spectroscopic probing is quite challenging,³² solution phase NCs can be readily subjected to any spectroscopic characterization.^{33–37} In addition, solution phase syntheses can be readily scaled up (e.g., milligrams to grams³⁸). The creation of size-discrete NCs in the protected form opens up opportunities for probing the properties of the nascent metallic state and metallic bond formation in ultrasmall NCs.^{39–41}

In this work, we report the cryogenic spectroscopic probing of whether the nascent metallic state in gold NPs is temperature dependent or not by utilizing atomically precise gold NCs. Two sizes, Au₂₇₉(SR)₈₄ and Au₃₃₃(SR)₇₉, are selected for this study, together with a nonmetallic Au₁₄₄(SR)₆₀ NC for comparison. Surprisingly, although the gaps of Au₂₇₉ and Au₃₃₃ are of $\sim k_B T$ at room temperature ($k_B T$ at r.t. ~ 25 meV), no effect on plasmon resonance from the transition to an insulating state at cryogenic temperatures is observed by monitoring the SPR (a signature of the electron-gas), even when the temperature is decreased to 2.5 K (i.e., ~ 0.2 meV), at which the E_g is already >100 times larger than the NC's thermal energy (i.e., nonmetallicity by eqn (5)). Based on the result, we further discuss some insights into metallic bond formation and nascent plasmon resonance emerged from coherent excitons.

Results and discussion

The Au₁₄₄(PET)₆₀ and Au₃₃₃(PET)₇₉ NCs (where PET = SCH₂-CH₂Ph) were synthesized by a size-focusing methodology reported in our previous work.^{40,42,43} Briefly, a narrow size-distributed Au_x(PET)_y mixture was first synthesized following the method of kinetic control, and such a crude product was then subject to size-focusing (e.g. thermal reaction with excess PET thiol at 80 °C for 2 days). The resulting Au₁₄₄ and Au₃₃₃ were separated by thin-layer chromatography (TLC, with CH₂Cl₂/methanol (6 : 1, v/v) as the eluent). The Au₂₇₉(TBBT)₈₄ (where TBBT = S-Ph-*p*-C(CH₃)₃) was synthesized by the ligand exchange-induced size transformation method.^{40,44} More experimental details, including the characterization, are provided in the ESI.†

Mass spectrometry and room temperature optical spectroscopy analyses

The high purity of the three NCs is confirmed by matrix-assisted laser desorption ionization (MALDI) and electrospray ionization (ESI) mass spectrometry analyses. As can be seen in Fig. 1A, MALDI analyses show a narrow peak at ~ 35 kDa for Au₁₄₄(PET)₆₀ and a ~ 75 kDa peak for Au₃₃₃(PET)₇₉, whereas the MALDI spectrum of Au₂₇₉(TBBT)₈₄ shows a 1+ charged peak at ~ 65 kDa (intense) and also a 2+ peak at ~ 32.5 kDa (weak). No impurity was observed in the wide-range MALDI spectra. The precise masses of the NCs were determined by ESI-MS (Fig. 1B). The Au₁₄₄(PET)₆₀ spectrum shows two dominant peaks of molecular ions at m/z 9149 (M^{4+}) and 12 199 (M^{3+}), plus a minor peak at 18 297 corresponding to the 2+ ion [Au₁₄₄(PET)₆₀]²⁺. These ions are formed under the ESI conditions, as the native state is charge-neutral. All three peaks are consistent with the expected formula weight of Au₁₄₄(PET)₆₀ (FW = 36 597.48 Da). The Au₂₇₉(TBBT)₈₄ (FW = 68 835.77 Da) spectrum shows peaks at m/z 17 209 (4+) and 22 945 (3+); note that the 2+ and 1+ peaks are beyond the mass detector's range and species of higher charges are not observed due to much less abundances under our ESI conditions. Finally, the ESI spectrum of Au₃₃₃(PET)₇₉ (FW = 76 430.23 Da) shows predominant mass peaks at m/z 15 286 (5+) and 19 108 (4+). The three NCs are all charge neutral in their native state.

The UV-vis absorption spectrum of Au₁₄₄ (dissolved in CH₂Cl₂) exhibits multiple peaks at 337, 463, 517, and 700 nm (Fig. 2A), consistent with previous reports.^{43,45} It is worth noting that Au₁₄₄ shows extra peaks in the near-infrared (NIR) range (ESI Fig. S1†). The multi-peak feature indicates the nonmetallic state of Au₁₄₄, that is, Au₁₄₄ possesses discrete electronic energy levels and gives rises to single-electron transitions (excitons), much like small molecules. Recent electrochemical measurements on Au₁₄₄ indeed revealed a 0.17 eV HOMO–LUMO gap at room temperature (r.t.),⁴⁶ and the gap became slightly larger with decreasing temperature, resembling the semiconductor behavior.³³ In contrast, Au₂₇₉ and Au₃₃₃ both show a nascent SPR peak at ~ 500 nm (Fig. 2B and C),^{40,47} and no measurable gap was observed in electrochemical measurements.⁴⁶ According to the independent-electron theory (eqn (4)), there should



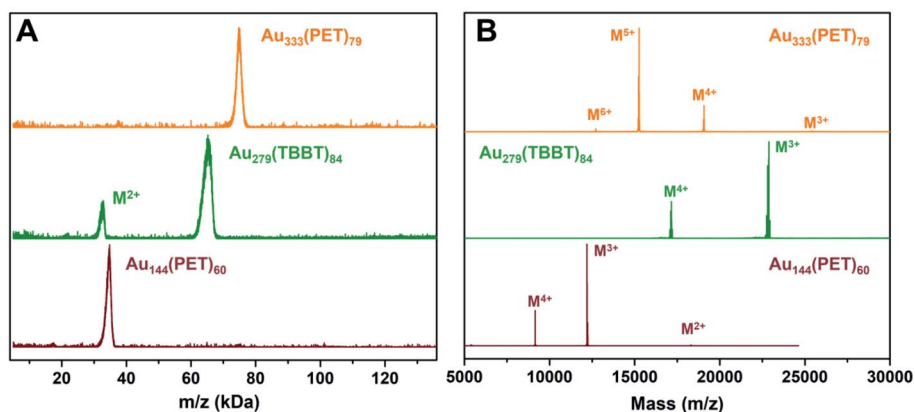


Fig. 1 Mass spectrometry characterization of $\text{Au}_{144}(\text{PET})_{60}$, $\text{Au}_{279}(\text{TBBT})_{84}$ and $\text{Au}_{333}(\text{PET})_{79}$, (A) MALDI mass spectra; (B) ESI mass spectra. In both the MALDI and ESI analyses, the neutral NCs become singly and/or multiply charged after ionization.

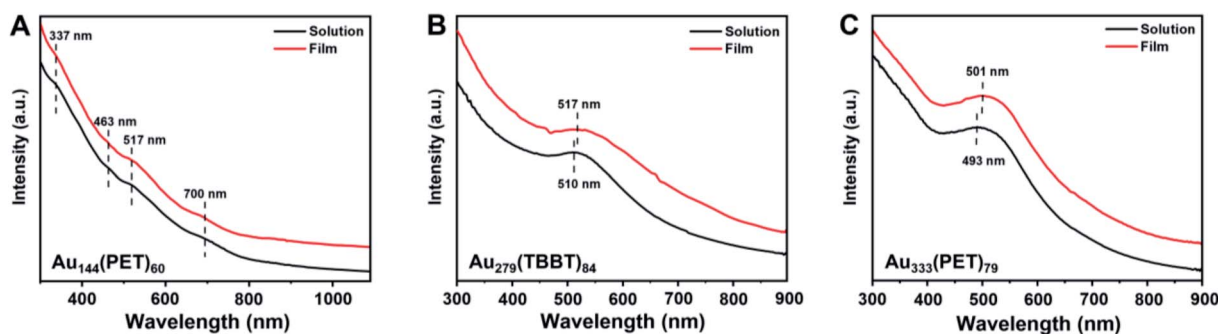


Fig. 2 Room temperature optical absorption spectra of (A) $\text{Au}_{144}(\text{PET})_{60}$, (B) $\text{Au}_{279}(\text{TBBT})_{84}$, and (C) $\text{Au}_{333}(\text{PET})_{79}$ in the solid film and solution, respectively.

be an ultrasmall gap in metallic Au_{279} and Au_{333} , as well as nonmetallic $\text{Au}_{246}(\text{SR})_{80}$ (its nonmetallicity confirmed by ultrafast spectroscopy analyses⁴⁸), since they are finite systems. However, ultrasmall gaps (*e.g.* at the meV scale or $k_{\text{B}}T$) is beyond the detection limit of electrochemical and spectroscopic measurements.^{46,48} Perhaps scanning tunneling spectroscopy at cryogenic temperatures or even millikelvin temperatures (*e.g.* using a dilution refrigerator as in quantum computing systems) may permit the measurement of the meV gaps.

Cryogenic spectroscopy probing of NCs down to 2.5 K

To test the possible temperature dependence of the nascent metallic state, we carried out cryogenic optical spectroscopy measurements (from r.t. down to 2.5 K). On that note, the cuvette-based measurement was only successful down to ~ 70 K but failed at lower temperatures due to shattering of cuvettes (even the cryogenic compatible ones), thus we switched to the thin-film based measurement for temperatures down to 2.5 K. The NCs are uniformly embedded in polystyrene thin films to acquire high quality spectra. At r.t., the film's optical spectra are almost superimposable to the solution spectra (Fig. 2A–C), albeit with a slight broadening of peaks. A sub-10 nm shift of absorption maxima is observed in Au_{279} and Au_{333} , whereas the peak shift in Au_{144} is trivial. For nonmetallic Au_{144} , the

difference between the solid film and the solution spectra can be ascribed to the coupling of electronic states with extra vibrational states induced by stronger inter-molecular interactions in the film state; whereas for Au_{279} and Au_{333} , a redshift of SPR is caused by the larger dielectric constant of the film, and a slight broadening of SPR due to accelerated ultrafast electron dynamics.⁶

The absorption spectra of the three film samples from r.t. down to 2.5 K are shown in Fig. 3A–C. For nonmetallic $\text{Au}_{144}(\text{PET})_{60}$, the bands at 517 nm and 700 nm clearly show a blueshift and become sharpened as the temperature decreases from r.t. to 2.5 K, and the peak shift fitting^{49,50} reveals a 15 meV vibrational mode coupled with the 700 nm peak, indicating a significant contribution of electron-phonon interaction. This phenomenon disagrees with Kubo and Kreibig's earlier prediction, *i.e.*, they believed that the electron-phonon scattering should be suppressed in small-sized NPs (*e.g.* the number of Au atoms < 240).⁵¹ An explanation for this contradiction is that the interaction between the metal core and the protecting ligands provides an extra energy relaxation pathway. In our measurements, several new features appear in the absorption spectrum of $\text{Au}_{144}(\text{PET})_{60}$ at cryogenic temperatures, which provides strong evidence for the discrete energy levels in $\text{Au}_{144}(\text{PET})_{60}$, consistent with the cryogenic measurements by



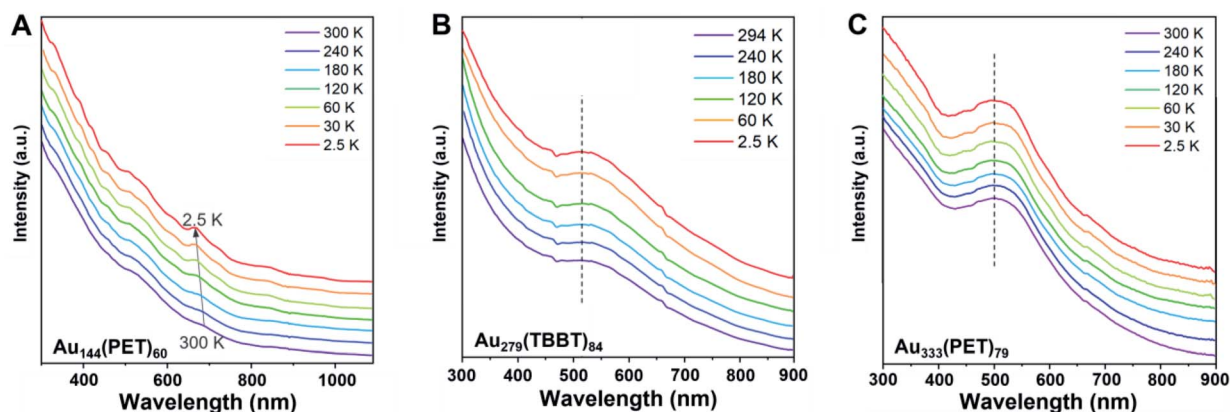


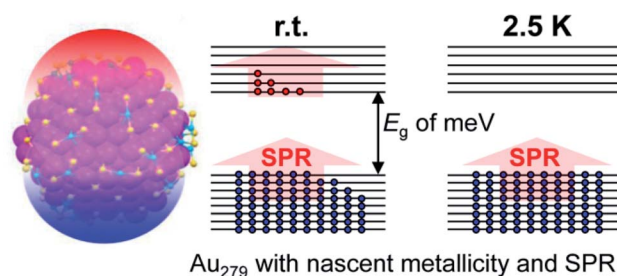
Fig. 3 Cryogenic optical absorption spectra of (A) $\text{Au}_{144}(\text{PET})_{60}$, (B) $\text{Au}_{279}(\text{TBBT})_{84}$, and (C) $\text{Au}_{333}(\text{PET})_{79}$ in solid films (r.t. to 2.5 K, NCs being embedded in thin films of polystyrene).

Weissker and Negishi *et al.* (their temperatures were only down to tens of kelvins).^{52,53} In contrast, the SPR peak of metallic-state $\text{Au}_{333}(\text{PET})_{79}$ and $\text{Au}_{279}(\text{TBBT})_{84}$ NCs shows no shift, except for a small increase in intensity and a negligible narrowing of bandwidth with the temperature down to 2.5 K. Similar trends were previously observed in larger sized, polydispersed Au NPs.⁵¹

It is interesting to observe no effect on the nascent SPR in $\text{Au}_{333}(\text{PET})_{79}$ and $\text{Au}_{279}(\text{TBBT})_{84}$ with their transition from the metallic to insulating state over the temperature decrease from r.t. to 2.5 K. We note that a temperature-dependent transition in a single La@C_{60} cluster was reported,⁵⁴ in which the scanning tunneling measurements of current–voltage (I – V) curves of La@C_{60} on graphite revealed a metal-to-semiconductor transition at 28 K, with the semiconducting state having a 40 meV gap. Of course, a major difference in our system is that the $\text{Au}_{333}(\text{PET})_{79}$ and $\text{Au}_{279}(\text{TBBT})_{84}$ NCs are optically excited (*i.e.* much higher excitation energy than the ultrasmall meV gaps).

Here we estimate the E_g of the three NCs by using the Kubo formula, E_f/N (note: the factor of 4/3 is dropped for estimation purposes). The first estimation takes all the gold atoms in the particle to be the N value in the Kubo formula (Table 1), while the second estimation takes the difference between the number of gold atoms and the number of ligands under the assumption that each thiolate ligand consumes one valence electron of gold in forming the Au–S covalent bond. The E_g values are compiled in Table 1, from which the case of Au_{144} shows a deviation of a factor of ~ 2 when compared with the experimental value, while there is no accurately measured E_g of Au_{279} and Au_{333} for

a comparison. The estimated E_g of Au_{279} and Au_{333} are comparable to the r.t. thermal energy (0.025 eV), which seems to explain the observed SPR and metallicity at r.t., because the r.t. thermal energy can effectively excite the free valence electrons to form an electron-gas. However, when the temperature is decreased, the electron-gas state would be destroyed since the electrons can no longer be excited thermally (Scheme 1); for example, at 2.5 K, the thermal energy is only ~ 0.0002 eV, about 150 times smaller than the E_g values (~ 0.03 eV for Au_{279} and Au_{333}), and thus it would be impossible to stir up the orbital-held electrons into an electron-gas. Therefore, one expects that the Au_{333} and Au_{279} transition to an insulating state at 2.5 K (Scheme 1), and accordingly it would exert some effects on the SPR, but no change to SPR was observed in our cryogenic probing. This implies that both Au_{279} and Au_{333} NCs, albeit with



Scheme 1 Thermal excitation of electrons and the nascent plasma state in Au_{279} . The block arrow represents plasmon excitation as opposed to single-electron (excitonic) excitation by incident light.

Table 1 Estimated E_g of Au_{144} , Au_{279} and Au_{333} (the E_f energy of bulk gold is taken as 5.5 eV)^a

	$\text{Au}_{144}(\text{SR})_{60}$ (1.7 nm core)	$\text{Au}_{279}(\text{SR})_{84}$ (2.2 nm)	$\text{Au}_{333}(\text{SR})_{79}$ (2.3 nm)
E_g by taking the total number of gold atoms	0.038 eV	0.020 eV	0.016 eV
E_g by taking the number of gold atoms subtracting the number of ligands	0.065 eV	0.028 eV	0.022 eV
Experimental E_g at r.t.	0.17 eV	n.d.	n.d.

^a n.d. = not determined, *i.e.* beyond the detection limit of electrochemical analyses.



a nonzero HOMO–LUMO gap of \sim meV, can sustain the plasma state (*i.e.* the electron-gas) without thermal contribution (Scheme 1).

The one-electron treatment adopts a free-electron-gas model and does not consider the electron–electron and electron–ion interactions.²⁶ A higher order theory (*e.g.* the Fermi liquid model^{26,55}) might be able to provide more insights into the temperature-dependent metallic/insulating states in finite systems. The above cryogenic spectroscopy result implies a nonthermal origin for electron-gas formation. When the energy level spacing is on the meV scale, the broadening of energy-levels should be taken into consideration, and the potential factors are the excited state lifetime-induced broadening, electron–phonon coupling, electronic structure renormalization upon excitation, *etc.*, all being on the meV scale, so that the meV HOMO–LUMO gap becomes smeared out, even in the absence of thermal excitation. In previous theoretical modeling using density functional theory (DFT), some researchers reported that the plasmon state would be formed in Au₁₄₄ and even the smaller Au₁₃₃ NC,^{56,57} but recent careful measurements do not support the theory because of the distinct gaps observed in these two NCs.⁴⁶ In addition, both NCs also showed molecular-like electron dynamics,³³ as well as luminescence,⁴⁶ hence, they are not in the metallic state. For large sizes of NCs (*e.g.* more than one hundred atoms of gold), it is still a major challenge to perform DFT analysis with sufficient accuracy. Thus, developing new methods is highly desired, and such efforts will contribute to addressing the fundamentals of metallic-state formation with increasing size.^{58,59}

Origin of nascent SPR

Here we further discuss the evolution of E_g and optical absorption spectra of gold nanoclusters with increasing size (Fig. 4). Smaller NCs ($n < 100$ or so) possess distinct E_g , such as Au₁₀₃ with a 0.4 eV gap (Fig. 4, green curve). In our recent work we observed a sharp transition from nonmetallic Au₂₄₆(SR)₈₀ to metallic Au₂₇₉(SR)₈₄.⁴⁰ The Au₂₄₆ NC exhibits multiple peaks (*i.e.* multi-excitons) as revealed in both the steady-state and femto-second transient absorption spectra, and its ultrafast electron relaxation dynamics showed no excitation power dependence, but with a mere 33-atom increase, the excitonic picture disappeared in Au₂₇₉ — which exhibited a single SPR peak at \sim 500 nm and power dependence in ultrafast electron dynamics.⁴⁰ It seems that the excitons in NCs larger than Au₂₄₆ start to “communicate” and develop a coherence, and the concerted excitonic transitions are generated and manifested as a plasmon excitation in Au₂₇₉ (Fig. 4). The development of such coherence and oscillator energy merging into SPR energy (\sim 2.5 eV) is intriguing (Fig. 4, comparing the Au₂₄₆ and Au₂₇₉ spectra).

In small NCs, a long-range electron–electron repulsion is present, *i.e.* $\frac{e^2}{r}$ (where e is the electron charge and r is the distance). With increasing size, the electronic screening effect builds up and leads to weak short-range forces, *i.e.* $\frac{e^2}{r} \exp\left(-\frac{r}{l}\right)$, where l is the screening length which is dependent on the

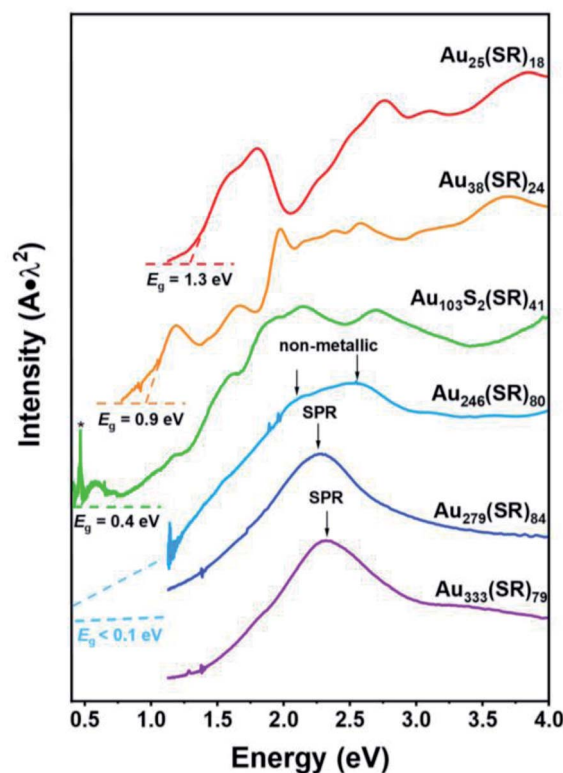


Fig. 4 Evolution of E_g and optical absorption spectra with size increasing from Au₂₅ to Au₃₃₃ (the asterisk at \sim 0.4 eV indicates the solvent's vibrational overtone absorption peak. Solvents: CH₂Cl₂ for the UV-vis range, CCl₄ for the UV-vis-NIR range. Temperature: r.t.).

electronic density (*i.e.* the higher the electronic density, the shorter the l , hence, the electron's Coulomb interaction becomes short-ranged). Ultimately, the strong screening effect leads to the formation of nearly independent electrons (*i.e.* the electron-gas). From the optical absorption spectra, we observed that in NCs larger than Au₁₀₃, long-wavelength absorption with relatively large oscillator strength starts to retreat toward shorter wavelengths (Fig. 4), indicating the excitons' peak energy focusing. The free propagation or ‘roaming’ of electrons in larger NCs such as Au₂₄₆ leads to stronger electronic screening, hence the merging of various excitons, and finally, giving rise to plasmonic excitation in Au₂₇₉. It remains to be elucidated whether the concerted excitonic excitations are solely induced by the increased electronic density with increasing size, or involve some other subtle factors. Heteroatom doping of Au₂₇₉ might provide more insights.

From the experiments, gold NCs with an ultras-small E_g of \sim 0.02–0.03 eV (comparable to $k_B T$ at r.t.) seem to already reach the metallic state or metallic bonding. Both Au₂₇₉ and Au₃₃₃ should transition to an insulating state at 2.5 K according to the Kubo criterion, albeit no effect on SPR is observed in cryogenic spectroscopic probing. The nonzero E_g in finite-sized Au₂₇₉ and Au₃₃₃ NCs is in contrast to bulk metals in which $E_g = 0$. In future work, it would be worthwhile to carry out far-infrared and terahertz absorption measurements to directly probe the ultras-small E_g , as opposed to the high energy excitation in UV-vis-NIR



spectroscopy analysis. Future theoretical work may also reveal more insights into the birth of coherence among the valence electrons with a build-up of electronic screening, the emergence of nascent plasmon resonances, and also the new properties of nascent plasmons.

Conclusions

In summary, cryogenic spectroscopy of Au₂₇₉ and Au₃₃₃ in the size domain (2.2 to 2.5 nm) provides insights into the temperature effect on the metallic state or metallic bonding in ultra-small particles. Au₂₇₉ and Au₃₃₃ show nascent metallicity at r.t. by exhibiting collective excitation of electrons (*i.e.* SPR), but no effect on SPR is observed from the metal-to-insulator transition ($E_g \gg k_B T$) when the temperature is decreased to 2.5 K, at which the thermal energy ($k_B T = 0.0002$ eV) is already significantly smaller than the estimated Kubo gaps (0.02–0.03 eV) of Au₂₇₉ and Au₃₃₃. The sustained electron-gas state in these ultrasmall NPs from r.t. down to 2.5 K implies a nonthermal mechanism for electron-gas formation. The electronic density-dependent screening of Coulomb repulsions between electrons leads to the formation of short-ranged electronic interactions with increasing size, hence, the development of an electron-gas. The coherence among excitons leads to the birth of SPR. The obtained insights contribute to the understanding of the fundamental metallic bond formation and electronic interactions, and also benefit the future applications of nanocluster materials in solar energy conversion, plasmonics, photocatalysis, sensing, and other fields.

Data availability

All the data have been included in the ESI.†

Author contributions

X. D. and T. H. performed the synthesis, Z. L. carried out cryogenic spectroscopy measurements, M. Z. collected some of the r.t. spectra, and R. J. designed the project. All authors discussed the results and contributed to the manuscript writing.

Conflicts of interest

There are no conflicts to declare.

Acknowledgements

R. J. is thankful for the financial support from the National Science Foundation (DMR-1808675).

References

- 1 Y. W. C. Cao, R. Jin and C. A. Mirkin, Nanoparticles with Raman Spectroscopic Fingerprints for DNA and RNA Detection, *Science*, 2002, **297**, 1536–1540.
- 2 R. Jin, C. Zeng, M. Zhou and Y. Chen, Atomically Precise Colloidal Metal Nanoclusters and Nanoparticles: Fundamentals and Opportunities, *Chem. Rev.*, 2016, **116**, 10346–10413.
- 3 G. V. Hartland, L. V. Besteiro, P. Johns and A. O. Govorov, What's So Hot about Electrons in Metal Nanoparticles?, *ACS Energy Lett.*, 2017, **2**, 1641–1653.
- 4 A. Arbouet, C. Voisin, D. Christofilos, P. Langot, N. Del Fatti, F. Vallée, J. Lermé, G. Celep, E. Cottancin, M. Gaudry, M. Pellarin, M. Broyer, M. Maillard, M. P. Pileni and M. Treguer, Electron-Phonon Scattering in Metal Clusters, *Phys. Rev. Lett.*, 2003, **90**, 177401.
- 5 X. Li, S. Takano and T. Tsukuda, Ligand Effects on the Hydrogen Evolution Reaction Catalyzed by Au₁₃ and Pt@Au₁₂: Alkynyl vs. Thiolate, *J. Phys. Chem. C*, 2021, **125**, 23226–23230.
- 6 M. Zhou, T. Higaki, G. Hu, M. Y. Sfeir, Y. Chen, D.-e. Jiang and R. Jin, Three-orders-of-magnitude variation of carrier lifetimes with crystal phase of gold nanoclusters, *Science*, 2019, **364**, 279–282.
- 7 M. Hesari, H. Ma and Z. F. Ding, Monitoring single Au₃₈ nanocluster reactions *via* electrochemiluminescence, *Chem. Sci.*, 2021, **12**, 14540–14545.
- 8 Z. Wang, H. T. Sun, M. Kurmoo, Q.-Y. Liu, G.-L. Zhuang, Q.-Q. Zhao, X.-P. Wang, C.-H. Tung and D. Sun, Carboxylic acid stimulated silver shell isomerism in a triple core-shell Ag₈₄ nanocluster, *Chem. Sci.*, 2019, **10**, 4862–4867.
- 9 M. H. Naveen, R. Khan, M. A. Abbas, E. Cho, G. J. Lee, H. Kim, E. Sim and J. H. Bang, Modulation of the photoelectrochemical behavior of Au nanocluster-TiO₂ electrode by doping, *Chem. Sci.*, 2020, **11**, 6248–6255.
- 10 T. Higaki, Q. Li, M. Zhou, S. Zhao, Y. Li, S. Li and R. Jin, Toward the Tailoring Chemistry of Metal Nanoclusters for Enhancing Functionalities, *Acc. Chem. Res.*, 2018, **51**, 2764–2773.
- 11 K. K. Chakrahari, R. P. B. Silalahi, J.-H. Liao, S. Kahlal, Y.-C. Liu, J.-F. Lee, M.-H. Chiang, J.-Y. Saillard and C. W. Liu, Synthesis and structural characterization of inverse-coordination clusters from a two-electron superatomic copper nanocluster, *Chem. Sci.*, 2018, **9**, 6785–6795.
- 12 C. M. Aikens, Electronic and Geometric Structure, Optical Properties, and Excited State Behavior in Atomically Precise Thiolate-Stabilized Noble Metal Nanoclusters, *Acc. Chem. Res.*, 2018, **51**, 3065–3073.
- 13 R. R. Nasaruddin, T. Chen, N. Yan and J. Xie, Roles of Thiolate Ligands in The Synthesis, Properties and Catalytic Application of Gold Nanoclusters, *Coord. Chem. Rev.*, 2018, **368**, 60–79.
- 14 X. Kang and M. Zhu, Tailoring the Photoluminescence of Atomically Precise Nanoclusters, *Chem. Soc. Rev.*, 2019, **48**, 2422–2457.
- 15 C. Zeng, Y. Chen, K. Kirschbaum, K. J. Lambright and R. Jin, Emergence of Hierarchical Structural Complexities in Nanoparticles and Their Assembly, *Science*, 2016, **354**, 1580–1584.
- 16 Y. Li, M. Zhou, Y. Song, T. Higaki, H. Wang and R. Jin, Double-Helical Assembly of Heterodimeric Nanoclusters into Supercrystals, *Nature*, 2021, **594**, 380–384.



- 17 G. Yousefalizadeh, S. Ahmadi, N. J. Mosey and K. G. Stamplecoskie, Exciting clusters, what does off-resonance actually mean?, *Nanoscale*, 2021, **13**, 242–252.
- 18 M. Shabaninezhad, A. Abuhagr, N. A. Sakthivel, C. Kumara, A. Dass, K. Kwak, K. Pyo, D. Lee and G. Ramakrishna, Ultrafast Electron Dynamics in Thiolate-Protected Plasmonic Gold Clusters: Size and Ligand Effect, *J. Phys. Chem. C*, 2019, **123**, 13344–13353.
- 19 P. Maioli, T. Stoll, H. E. Saucedo, I. Valencia, A. Demessence, F. Bertorelle, A. Crut, F. Vallée, I. L. Garzón, G. Cerullo and N. Del Fatti, Mechanical Vibrations of Atomically Defined Metal Clusters: From Nano- to Molecular-Size Oscillators, *Nano Lett.*, 2018, **18**, 6842–6849.
- 20 W. W. Xu, Y. Li, Y. Gao and X. C. Zeng, Unraveling a Generic Growth Pattern in Structure Evolution of Thiolate-Protected Gold Nanoclusters, *Nanoscale*, 2016, **8**, 7396–7401.
- 21 Y. Pei, P. Wang, Z. Ma and L. Xiong, Growth-Rule-Guided Structural Exploration of Thiolate-Protected Gold Nanoclusters, *Acc. Chem. Res.*, 2019, **52**, 23–33.
- 22 Z. Lei, J.-J. Li, X.-K. Wan, W.-H. Zhang and Q.-M. Wang, Isolation and Total Structure Determination of an All-Alkynyl-Protected Gold Nanocluster Au₁₄₄, *Angew. Chem., Int. Ed.*, 2018, **57**, 8639–8643.
- 23 M. C. Heaven, V. E. Bondybej, J. M. Merritt and A. L. Kaledin, The Unique Bonding Characteristics of Beryllium and the Group IIA Metals, *Chem. Phys. Lett.*, 2011, **506**, 1–14.
- 24 D. A. Tomalia and S. N. Khanna, A Systematic Framework and Nanoperiodic Concept for Unifying Nanoscience: Hard/Soft Nanoelements, Superatoms, Meta-Atoms, New Emerging Properties, Periodic Property Patterns, and Predictive Mendeleev-like Nanoperiodic Tables, *Chem. Rev.*, 2016, **116**, 2705–2774.
- 25 R. Jin, Quantum sized, Thiolate-Protected Gold Nanoclusters, *Nanoscale*, 2010, **2**, 343–362.
- 26 R. Kubo, Electronic Properties of Small Particles, *Annu. Rev. Mater. Sci.*, 1984, **14**, 49–66.
- 27 U. Kreibitz and M. Vollmer, *Optical Properties of Metal Clusters*, Springer-Verlag, New York, 1995.
- 28 B. von Issendorff and O. Cheshnovsky, Metal to Insulator Transitions in Clusters, *Annu. Rev. Phys. Chem.*, 2005, **56**, 549–580.
- 29 H. Haberland, B. von Issendorff, Y. Ji and T. Kolar, Transition to Plasmonlike Absorption in Small Hg Clusters, *Phys. Rev. Lett.*, 1992, **69**, 3212–3215.
- 30 J. Wang, G. Wang and J. Zhao, Nonmetal–Metal Transition in Zn_n ($n = 2 - 20$) Clusters, *Phys. Rev. A*, 2003, **68**, 013201.
- 31 Y. Jiang, K. Wu, J. Ma, B. Wu, E. G. Wang and P. Ebert, Quantum Size Effects in the Nonmetal to Metal Transition of Two-Dimensional Al Islands, *Phys. Rev. B: Condens. Matter Mater. Phys.*, 2007, **76**, 235434.
- 32 A. Cirri, H. M. Hernández, C. Kmiotek and C. J. Johnson, Systematically Tuning the Electronic Structure of Gold Nanoclusters through Ligand Derivatization, *Angew. Chem., Int. Ed.*, 2019, **58**, 13818–13822.
- 33 M. Zhou and R. Jin, Optical Properties and Excited-State Dynamics of Atomically Precise Gold Nanoclusters, *Annu. Rev. Phys. Chem.*, 2021, **72**, 121–142.
- 34 F. Hu, Z.-J. Guan, G. Yang, J.-Q. Wang, J.-J. Li, S.-F. Yuan, G.-J. Liang and Q.-M. Wang, Molecular Gold Nanocluster Au₁₅₆ Showing Metallic Electron Dynamics, *J. Am. Chem. Soc.*, 2021, **143**, 17059–17067.
- 35 T. Zhao, P. J. Herbert, H. Zheng and K. L. Knappenberger Jr, State-Resolved Metal Nanoparticle Dynamics Viewed through the Combined Lenses of Ultrafast and Magneto-optical Spectroscopies, *Acc. Chem. Res.*, 2018, **51**, 1433–1442.
- 36 G. Yousefalizadeh and K. G. Stamplecoskie, A Single Model for the Excited-State Dynamics of Au₁₈(SR)₁₄ and Au₂₅(SR)₁₈ Clusters, *J. Phys. Chem. A*, 2018, **122**, 7014–7022.
- 37 T. Higaki, C. Liu, D. J. Morris, G. He, T.-Y. Luo, M. Y. Sfeir, P. Zhang, N. L. Rosi and R. Jin, Au_{130-x}Ag_x Nanoclusters with Non-Metallicity: A Drum of Silver-Rich Sites Enclosed in a Marks-Decahedral Cage of Gold-Rich Sites, *Angew. Chem., Int. Ed.*, 2019, **131**, 18974–18978.
- 38 Y. Song, K. Lambright, M. Zhou, K. Kirschbaum, J. Xiang, A. Xia, M. Zhu and R. Jin, Large-Scale Synthesis, Crystal Structure, and Optical Properties of the Ag₁₄₆Br₂(SR)₈₀ Nanocluster, *ACS Nano*, 2018, **12**, 9318–9325.
- 39 M. Zhou, C. Zeng, Y. Chen, S. Zhao, M. Y. Sfeir, M. Zhu and R. Jin, Evolution from the Plasmon to Exciton State in Ligand-Protected Atomically Precise Gold Nanoparticles, *Nat. Commun.*, 2016, **7**, 13240.
- 40 T. Higaki, M. Zhou, K. J. Lambright, K. Kirschbaum, M. Y. Sfeir and R. Jin, Sharp Transition from Nonmetallic Au₂₄₆ to Metallic Au₂₇₉ with Nascent Surface Plasmon Resonance, *J. Am. Chem. Soc.*, 2018, **140**, 5691–5695.
- 41 N. A. Sakthivel, M. Stener, L. Sementa, A. Fortunelli, G. Ramakrishna and A. Dass, Au₂₇₉(SR)₈₄: The Smallest Gold Thiolate Nanocrystal That Is Metallic and the Birth of Plasmon, *J. Phys. Chem. Lett.*, 2018, **9**, 1295–1300.
- 42 H. Qian, Y. Zhu and R. Jin, Atomically Precise Gold Nanocrystal Molecules with Surface Plasmon Resonance, *Proc. Natl. Acad. Sci. U. S. A.*, 2012, **109**, 696–700.
- 43 H. Qian and R. Jin, Controlling Nanoparticles with Atomic Precision: The Case of Au₁₄₄(SCH₂CH₂Ph)₆₀, *Nano Lett.*, 2009, **9**, 4083–4087.
- 44 C. Zeng, Y. Chen, A. Das and R. Jin, Transformation Chemistry of Gold Nanoclusters: From One Stable Size to Another, *J. Phys. Chem. Lett.*, 2015, **6**, 2976–2986.
- 45 N. Yan, N. Xia, L. Liao, M. Zhu, F. Jin, R. Jin and Z. Wu, Unraveling the Long-Pursued Au₁₄₄ Structure by X-Ray Crystallography, *Sci. Adv.*, 2018, **4**, eaat7259.
- 46 S. Chen, T. Higaki, H. Ma, M. Zhu, R. Jin and G. Wang, Inhomogeneous Quantized Single-Electron Charging and Electrochemical-Optical Insights on Transition-Sized Atomically Precise Gold Nanoclusters, *ACS Nano*, 2020, **14**, 16781–16790.
- 47 T. Higaki, M. Zhou, G. He, S. D. House, M. Y. Sfeir, J. C. Yang and R. Jin, Anomalous Phonon Relaxation in Au₃₃₃(SR)₇₉ Nanoparticles with Nascent Plasmons, *Proc. Natl. Acad. Sci. U. S. A.*, 2019, **116**, 13215–13220.
- 48 M. Zhou, C. Zeng, Y. Song, J. W. Padelford, G. Wang, M. Y. Sfeir, T. Higaki and R. Jin, On the Non-Metallicity of 2.2 nm Au₂₄₆(SR)₈₀ Nanoclusters, *Angew. Chem., Int. Ed.*, 2017, **129**, 16475–16479.



- 49 Z. Liu, Y. Li, W. Shin and R. Jin, Observation of Core Phonon in Electron-Phonon Coupling in Au₂₅ Nanoclusters, *J. Phys. Chem. Lett.*, 2021, **12**, 1690–1695.
- 50 M. S. Devadas, S. Bairu, H. Qian, E. Sinn, R. Jin and G. Ramakrishna, Temperature-Dependent Optical Absorption Properties of Monolayer-Protected Au₂₅ and Au₃₈ Clusters, *J. Phys. Chem. Lett.*, 2011, **2**, 2752–2758.
- 51 U. Kreibig, Anomalous Frequency and Temperature Dependence of the Optical Absorption of Small Gold Particles, *J. Phys., Colloq.*, 1977, **38**, C2-97–C2-103.
- 52 H.-C. Weissker, H. B. Escobar, V. D. Thanthirige, K. Kwak, D. Lee, G. Ramakrishna, R. L. Whetten and X. López-Lozano, Information on Quantum States Pervades the Visible Spectrum of the Ubiquitous Au₁₄₄(SR)₆₀ Gold Nanocluster, *Nat. Commun.*, 2014, **5**, 3785.
- 53 Y. Negishi, T. Nakazaki, S. Malola, S. Takano, Y. Niihori, W. Kurashige, S. Yamazoe, T. Tsukuda and H. Häkkinen, A Critical Size for Emergence of Nonbulk Electronic and Geometric Structures in Dodecanethiolate-Protected Au Clusters, *J. Am. Chem. Soc.*, 2015, **137**, 1206–1212.
- 54 R. Klingeler, G. Kann, I. Wirth, S. Eisebitt, P. S. Bechthold, M. Neeb and W. Eberhardt, La@C₆₀: A Metallic Endohedral Fullerene, *J. Chem. Phys.*, 2001, **115**, 7215–7218.
- 55 V. D. Borman, P. V. Borisyuk, V. V. Lebid'ko, M. A. Pushkin, V. N. Tronin, V. I. Troyan, D. A. Antonov and D. O. Filatov, A Study of Many-Body Phenomena in Metal Nanoclusters (Au, Cu) Close to Their Transition to the Nonmetallic State, *J. Exp. Theor. Phys.*, 2006, **102**, 303–313.
- 56 S. Malola, L. Lehtovaara, J. Enkovaara and H. Häkkinen, Birth of the Localized Surface Plasmon Resonance in Monolayer-Protected Gold Nanoclusters, *ACS Nano*, 2013, **7**, 10263–10270.
- 57 K. Iida, M. Noda and K. Nobusada, Interface Electronic Properties Between a Gold Core and Thiolate Ligands: Effects on an Optical Absorption Spectrum in Au₁₃₃(SPh-tBu)₅₂, *J. Phys. Chem. C*, 2016, **120**, 2753–2759.
- 58 L. Yang, P. Wang, Z. Yang and Y. Pei, Effect of Thiolate-Ligand Passivation on The Electronic Structure and Optical Absorption Properties of Ultrathin One and Two-Dimensional Gold Nanocrystals, *Nanoscale*, 2020, **12**, 5554–5566.
- 59 L. Xiong and Y. Pei, Evolution of Electronic Structure of Cuboid Thiolate-Monolayer-Protected Gold Nanocrystals, *J. Phys. Chem. C*, 2021, **125**, 20670–20675.

